Optical Mobile Communications: Principles, Implementation, and Performance Analysis

Zaichen Zhang, *Senior Member, IEEE*, Jian Dang, *Member, IEEE*, Liang Wu, *Member, IEEE*, Haibo Wang, *Member, IEEE*, Jun Xia, Wei Lei, Jiangzhou Wang, *Fellow, IEEE*, and Xiaohu You, *Fellow, IEEE*

***Abstract*—Owing to the rapid growth of mobile data communication and spectrum crunch at lower radio frequency, utilizing high frequency spectrum such as millimeter wave for ultra-high data rate mobile communications becomes necessary. Yet the propagation behaviors of high frequency radio waves make mobile communications rather challenging with a lot of technical problems, such as very large propagation loss. In this paper, we propose a novel approach, referred to as optical mobile communications (OMC), to cater to the need for high data rate mobile communication by exploiting optical beams. Taking spatial light modulator as an exemplary means of laser beam adaptation, we first present the system model of OMC. It is shown that the downlink channels in OMC are different from that in a system equipped with antennas emitting radio frequency signals. That is, the OMC channels for different mobile terminals are controllable to a large extent. This new feature creates a new dimension for performance optimization of OMC. We then investigate the achievable rate region of OMC using different multiple access schemes in a two-user downlink system. Numerical results show that expanded rate region can be achieved in OMC compared to the case where channels are not controllable, which shows the potential of OMC as a promising technique.**

***Index Terms*—Optical mobile communications, multiple access, achievable rate region, beam adaptation.**

I. Introduction

With the fast development of mobile communication systems (MCSs), radio spectrum has a limitation to provide extreme high throughput services [1]–[4]. On the other hand, optical spectrum can be explored and play a more and more important role in the next generation of MCSs [5], [6]. Besides having huge available bandwidth, an optical wireless signal is also capable of achieving near perfect energy concentration through directed beams, which is important in the development of a high throughput wireless communication system. Here "energy concentration" refers to focusing all the available transmit energy to the direction of desired receivers, without wasting energy propagated to other spatial areas. Achieving better energy concentration is an important development path of the MCSs. One example is adoption of smaller cells to restrict the transmit energy to smaller areas. Another example is using massive multiple-input multiple-output (MIMO) [7]–[10] technologies to achieve a narrower beamwidth, so that the energy can be transmitted to the desired receivers precisely.

Visible light communication (VLC) [11], [12] is a topic belonging to optical wireless communication (OWC). It has the advantage of utilizing the existing lighting infrastructure to provide ubiquitous wireless communication services. However, a typical VLC scheme is not "energy concentration". Light signal from the light-emitting diode (LED) source covers an area (we call the illuminated area) and performs lighting and signal transmission simultaneously. Due to the fact that the effective receiving area of the receiver is much smaller than the illuminated area, only a small fraction of the transmit energy is collected for communication purpose. Therefore, from the point view of "energy concentration", existing VLC schemes are not suitable for very high throughput and energy efficient transmissions.

Free space optical (FSO) [13] is a mature OWC approach. It is typically suitable for very high data rate point-to-point wireless transmissions. The transmit energy is concentrated on the direction of the receiver by adopting narrow laser beams. An acquisition, tracking, and pointing (ATP) subsystem [14] tracks the receiver adaptively if there is a tiny amount of position shift between the transmitter and the receiver. Unfortunately state-of-the-art FSO technologies cannot handle high-speed moving scenarios which is typical in an MCS.

To meet the need for next generation MCSs, optical mobile communication (OMC) was proposed recently [15]. Different from FSO, OMC supports multiple senders and multiple receivers, with possible high mobility and handover among cells. OMC achieves higher throughput and energy efficiency, and supports higher mobility than VLC. OMC is complementary

Manuscript received December 16, 2017; revised May 23, 2018 and September 6, 2018; accepted November 6, 2018. Date of publication November 12, 2018; date of current version January 15, 2019. This work was supported in part by the National Natural Science Foundation of China projects under Grants 61571105, 61501109, 61601119, and 61223001, and in part by Jiangsu National Science Foundation project under Grant BK20140646. The review of this paper was coordinated by Prof. J. F. Paris. *(Corresponding author: Zaichen Zhang.)*

Z. Zhang, J. Dang, L. Wu, H. Wang, and X. You are with the National Mobile Communications Research Laboratory, Quantum Information Research Center, Southeast University, Nanjing 210096, China (e-mail: zczhang@seu.edu.cn; dangjian@seu.edu.cn; wuliang@seu.edu.cn; haibowang@seu.edu.cn; xhyu@seu.edu.cn).

J. Xia and W. Lei are with the Joint International Research Laboratory of Information Display and Visualization, Southeast University, Nanjing 210096, China (e-mail: xiajun@seu.edu.cn; lw@seu.edu.cn).

J. Wang is with the School of Engineering and Digital Arts, University of Kent, Canterbury CT2 7NT, U.K. (e-mail: j.z.wang@kent.ac.uk).

This paper has supplementary downloadable material available at http://ieeexplore.ieee.org provided by the author.

Color versions of one or more of the figures in this paper are available online at http://ieeexplore.ieee.org.

Digital Object Identifier 10.1109/TVT.2018.2880817

to radio frequency (RF) wireless communication systems. It provides fiber-like high throughput wireless service when the optical wireless link is available. One of the typical applications of OMC is infrastructure-to-vehicle (I2V) networks, where access points at the roadside compose an access network and send high-speed data to mobile vehicles. Reverse link can also be constructed using the same technology. Another application of OMC is establishing dynamic laser connections in a mobile ad hoc network (MANET). Quantum key distribution (QKD) [16] is possible on the laser links to achieve quantum level security for the MANET when it serves as a tactical network such as in unmanned aerial vehicle (UAV) military communication. Compared with other promising techniques for high-speed mobile communication such as millimeter wave communication [17], OMC entitles abundant spectrum resource, very high energy efficiency, good electromagnetic compatibility, lower costs of hardware implementation, and easy combination with QKD. Therefore, OMC could be more attractive in future mobile communications with emphasis on ultra-high data rate, energy efficiency and quantum security.

There are several key design problems with OMC. One is the beam adaptation, i.e., how to allocate optical beams to one or multiple receivers and track the receivers adaptively in a potentially high-speed scenario. Beam adaptation also brings a new dimension of channel modeling, where the channel can be controllably dynamic, which is useful for obtaining better performance. In this paper, we propose a method for beam adaptation based on optical devices and units. We show the original beam can be split with adjustable power allocations and redirected to multiple users at different locations using the proposed method. Based on this, OMC is applied to a I2V communication scenario as an example to show how it works. In addition, the rate region is analyzed for OMC in a two-user case using different multiple access schemes and compared with existing OWC approach. Numerical results show that OMC has larger rate region than OWC which reveals its potential performance gain. Other possible ways of beam adaptation and feasibility issues are also discussed to confirm and expand this work. The contribution of this work can be summarized as follows:

- We elaborated the new concept of OMC which is originally proposed in [15]. We not only explained the concept in a more specific system setup (OMC for the on-road moving cars), but also provided a candidate implementation technique based on optical devices and units.
- We analyzed the rate performance of OMC and compared it with the conventional OWC. The results showed that expanded rate region could be achieved using OMC, which is new to existing literature.
- We conducted preliminary experiments in lab to show the concept of OMC and feasibility of beam adaptation.

This paper is organized as follows. In Section II, the system model is given. A beam adaptation scheme is proposed in Section III. Section IV gives the rate region analysis and comparison for a two-user downlink OMC system. Section V discusses some engineering issues related to the feasibility of OMC and points on several other problems for further research. Section VI concludes this paper.

Fig. 1. OMC based on I2V network.

II. System Model

Consider the system model of OMC based on the I2V network shown in Fig. 1. The same model can be applicable to other application scenarios. The basic requirement of the optical source is that it should be capable of splitting the laser beams and directing them to desired users adaptively. There are several ways to implement beam adaptation, which will be discussed in Section V. Among them, optical phased array (OPA) [18] has high flexibility and integration level, and is capable of splitting and steering optical beams with easy control. Therefore, we build the system model assuming that OPA is used for beam adaptation in OMC.

It is assumed that an access point (AP) in the I2V network is sending to N mobile terminals (MTs) in its cell through the optical wireless links. Let $u(t)$ be the aggregated RF signal of the N users to be sent, $u(t) = \sum_{i=1}^{N} u_i(t)$, where $u_i(t)$ is the RF signal of the ith user. $u(t)$ is modulated on a laser beam at AP. The modulated signal can be expressed as

$$s(t) = A_c A_u(t) \cos(2\pi f_c t + \theta_u(t) + \phi_0), \tag{1}$$

where A_c, f_c, and ϕ_0 are the amplitude, frequency, and initial phase of the optical carrier, respectively, $A_u(t)$ and $\theta_u(t)$ are the RF signal-dependent components of the modulated signal, depending on the modulation schemes used. For example, if phase modulation is adopted, $A_u(t) = 1$ and $\theta_u(t) = k_p u(t)$, where k_p is the phase modulation factor.

Assuming that the OPA has K phase-shift elements, each of which is able to add a phase shift ψ_k to the incident modulated optical signal independently, $\psi_k \in [0, 2\pi)$. The incident optical power to the kth element is p_k, which is normalized to the total incident power such that $0 \le p_k \le 1$ and $0 < \sum_{k=1}^{K} p_k \le 1$. Phase-shifted optical signal from the kth element is

$$s_k(t) = A_c \sqrt{p_k} A_u(t) \cos(2\pi f_c t + \theta_u(t) + \psi_k + \phi_0), \tag{2}$$

The received optical signal of the nth user can be written as

$$y_n(t) = \sum_{k=1}^{K} h_{n,k} s_k(t - \tau_{n,k}) + o_n(t)$$
$$= \sum_{k=1}^{K} h_{n,k} s_k(t - \tilde{\tau}_n - \delta_{n,k}) + o_n(t) \quad (3)$$

where $h_{n,k}$ and $\tau_{n,k}$ are the path gain and path delay from the kth element to the nth user, respectively. $o_n(t)$ is the additive optical noise at this user. $h_{n,k}, \tau_{n,k}$, and ψ_k have varying speeds much slower than that of the optical and RF signals, thus written as constant values here for simple analysis. $\tilde{\tau}_n = \frac{1}{K}\sum_{k=1}^{K} \tau_{n,k}$ is an average value of the path delay from the OPA to user n and $\delta_{n,k} = \tau_{n,k} - \tilde{\tau}_n$ is difference of the path delay of the kth element to the average value $\tilde{\tau}_n$. $\delta_{n,k}$ is related to distances of different OPA elements and typically at an order less than 10^{-11} seconds, which can be ignored for $A_u(t)$ and $\theta_u(t)$. Therefore, the received signal $y_n(t)$ can be written as

$$y_n(t) = \sum_{k=1}^{K} [h_{n,k} A_c \sqrt{p_k} A_u(t - \tilde{\tau}_n)$$
$$\times \cos(2\pi f_c(t - \tau_{n,k}) + \theta_u(t - \tilde{\tau}_n) + \psi_k + \phi_0)] + o_n(t) \quad (4)$$

From (4), the total phase change from the kth element to the nth user is

$$\beta_{n,k} = 2\pi f_c \tau_{n,k} + \psi_k \mod 2\pi \quad (5)$$

If $\{\psi_k, k = 1, 2, \ldots, K\}$ are set such that $\{\beta_{n,k}, k = 1, 2, \ldots, K\}$ have almost the same phase, i.e., $\beta_{n,k} \approx \beta_n, k = 1, 2, \ldots, K$, optical power will be aggregated at user n. In fact, as we will see in the next section, by tuning the phases $\{\psi_k, k = 1, 2, \ldots, K\}$ using a special signal (hologram) as an input to OPA to control the liquid crystals, it is also possible that the optical power is redirected to the N users simultaneously in an image plane with the aids of a lens system. In this more general case, each user shares a fraction of the total optical power. Therefore, $y_n(t)$ can be written as

$$y_n(t) = \sum_{k=1}^{K} [h_{n,k} A_c \sqrt{p_k} A_u(t - \tilde{\tau}_n)$$
$$\times \cos(2\pi f_c t + \theta_u(t - \tilde{\tau}_n) + \beta_n + \phi_0)] + o_n(t) \quad (6)$$

The RF signal $u(t)$ is then recovered by a coherent optical receiver, using a demodulation scheme matching the modulation scheme used by the AP. The recovered signal can be written as

$$\hat{u}_n(t) \approx q_n u(t) + w_n(t) \quad (7)$$

where q_n is related to $h_{n,k}, p_k, \beta_n$, and the receiving parameters of user n, and β_n is further determined by $\tau_{n,k}$ and ψ_k. $w_n(t)$ is an additive noise in the electrical domain. q_n can be assumed as a constant and viewed as the *effective* channel gain of user-n which represents the combined effects of energy concentration[1] through an optical system at the transmitter and the light propagation channel from transmitter to receiver. In the following, we will give an exemplary approach to implement the function of (6) and (7).

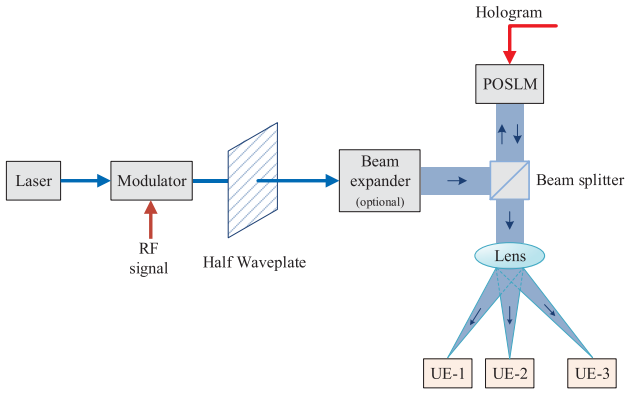

Fig. 2. Diagram of beam adaptation using LC-SLM.

III. Implementation of Beam Adaptation

Beam adaptation of OMC requires not only steering an optical beam to mobile users, but also distributing optical power to multiple users in a 2-dimension or 3-dimension environment dynamically. In this section, a feasible scheme based on liquid crystal spatial light modulator (LC-SLM) is investigated.

LC-SLM has been heavily investigated for beam steering [19], [20]. In OMC, we will use LC-SLM for beam adaptation with the help of a lens system. The system diagram is illustrated in Fig. 2.

The optical setup includes three core parts, i.e., the modulator, SLM, and lens system. The modulator modulates the RF signal on a laser beam. The modulated optical beam is then reflected by a phase-only SLM (POSLM). Here, the POSLM is a pixelated liquid crystal device driven by a silicon back plane. The liquid crystal is parallel aligned and it only modulates the phase of incident light received per crystal element. By doing so and with other designed mechanisms, SLM is capable of generating a desired complex light field $H(v_1, v_2; t) \triangleq s(t) f(v_1, v_2)$ by feeding it a pre-calculated static signal $f(v_1, v_2)$ where v_1 and v_2 denote the horizontal and vertical coordinates, respectively [21]. As a consequence, we can use a signal $f(v_1, v_2)$ to control SLM such that the reflected light energy is directed and concentrated to desired users only. However, using SLM for energy concentration based on $f(v_1, v_2)$ directly is not efficient due to the diffraction efficiency of SLM decreasing rapidly with increasing beam deflection angle [22]. In practice, a lens system can be employed between the SLM and the user plane to ease the problem. As Fig. 2 shows, the light field after SLM will be transformed to a different light field by the lens system and well projected on the user plane. In this regard, the user plane is also

[1]Note that the total energy is split among users and concentrate to desired users simultaneously.

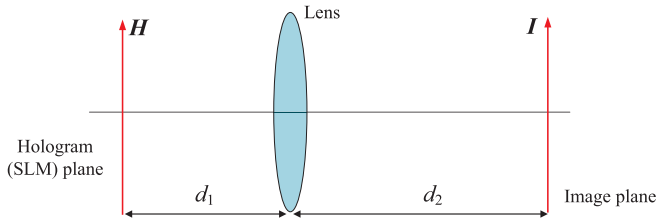

Fig. 3. Optical implementation of extended FRFT system.

referred to as image plane (I-plane) while the plane right after SLM is referred to as hologram plane (H-plane) and the signal $f(v_1, v_2)$ is referred to as hologram signal. The light propagation through the SLM and lens system can be described by the fractional Fourier transformation (FRFT), which will be detailed in the following.

The FRFT was first proposed by Namias [23] and it was expressed in one-dimension form. However, the definition widely used in the optics system for image projection was proposed by Lohmann based on the rotation of Wigner Distribution Function [24]–[26]. Later on, [27] extended the standard fractional Fourier into a more generalized optical system. The model of general optical projection system is plotted in Fig. 3, in which H and I represent the SLM hologram and image plane, respectively. Therefore, according to the extended fractional Fourier optics theory [28], the complex light field of plane H and I satisfies the fractional Fourier transform relation, i.e.,

$$I(\mu_1, \mu_2; t) = s(t)F(\mu_1, \mu_2) \tag{8}$$

where $I(\mu_1, \mu_2; t)$ is the complex light field of the image (user) plane with μ_1, μ_2 denoting the horizontal and vertical coordinates, respectively, and $F(\mu_1, \mu_2)$ is the extended fractional Fourier transform of the hologram signal $f(v_1, v_2)$ which is expressed by (9) at the bottom of this page. The parameters a, b, and ϕ are defined by

$$\begin{aligned} a^2 &= \frac{\sqrt{f-d_2}}{\lambda\sqrt{f-d_1}[f^2-(f-d_1)(f-d_2)]^{1/2}} \\ \phi &= \arccos\left(\frac{\sqrt{f-d_1}\cdot\sqrt{f-d_2}}{f}\right) \\ b^2 &= \frac{\sqrt{f-d_1}}{\lambda\sqrt{f-d_2}[f^2-(f-d_1)(f-d_2)]^{1/2}} \end{aligned} \tag{10}$$

where f is the focal length of the lens in the optical system, λ is the wavelength of the light, d_1 and d_2 are the distance from the lens to the hologram plane and image plane, respectively. Eq. (10) shows the relations between the parameters. That is, when the parameters, i.e., d_1, d_2, λ, and f in the optical projection system, are determined, the parameters of a, b, and ϕ can be calculated according to Eq. (10), then the light field propagation between the hologram and the image can be calculated by Eq. (8). As the distances measured from the lens to the H and I planes can be changed with different orders, in OMC, as long as the locations of users are known a priori, we are able to generate a desirable hologram for SLM through inverse FRFT such that the projected light (image) can be focused on the interested users' locations for efficient data transmission. In addition, the power splitting ratio $|q_n|^2$ among users can also be taken into account in the calculation of hologram signal $f(v_1, v_2)$. By this means, beam adaptation as well as energy concentration with *controllable* power allocation on interested users are realized as Eq. (7) shows.

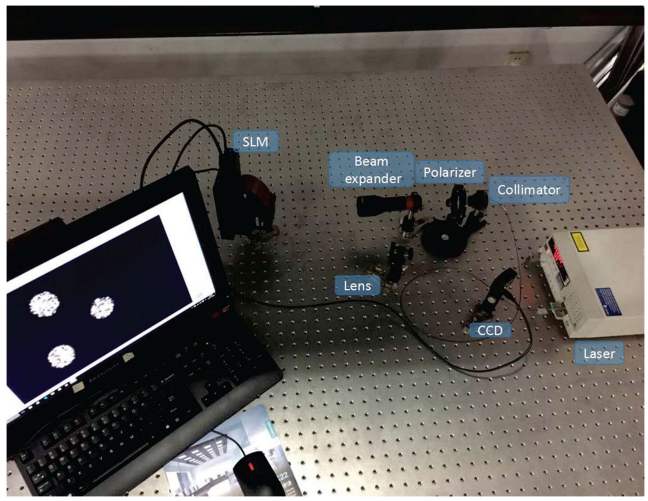

Fig. 4. Experimental setup of beam adaptation using a SLM.

To verify the feasibility of the proposed beam adaptation method, preliminary experiments are conducted in our lab. Fig. 4 illustrates an example of beam adaptation using a commercially available SLM (P1920-1550-HDMI, Meadowlark Optics). The experiment generates three optical beams from a single laser source of 1550 nm by feeding SLM a desirable hologram signal. The reflected beams from SLM are received using a charge-coupled device (CCD) camera and projected on the screen of a laptop. Using SLM, the beam could be flexibly tuned. Fig. 5 shows an CCD image generated by the experiment which shows the characters 'OMC'. As another example, an additional experiment with larger distance using 532 nm green light is shown in Fig. 6. A video clip showing moving green dots is also available as multimedia attachment of this paper. Those results show the proposed method can generate arbitrary beam "patterns", which is desired in the application of OMC.

For the dynamic response time of POSLM, since it uses the birefringence of liquid crystal material to tune the light path, the response time is mainly determined by the viscosity and the thickness of the liquid crystal layer. Lower viscosity and smaller thickness are preferred for faster response. However, for phase modulation of light, at least 2π phase range is required. The thickness (d) of the liquid crystal layer is therefore determined by the birefringence difference (Δ). That is $d \gg 2\pi\lambda/\Delta$. Since

$$F(\mu_1, \mu_2) = \int\int f(v_1, v_2) \exp\left[j\pi\left(\frac{a^2v_1^2 + v_2^2 + b^2\mu_1^2 + \mu_2^2}{\tan\phi} - \frac{2ab(v_1\mu_1 + v_2\mu_2)}{\sin\phi}\right)\right] dv_1 dv_2 \tag{9}$$

Fig. 5. CCD camera image generated by SLM.

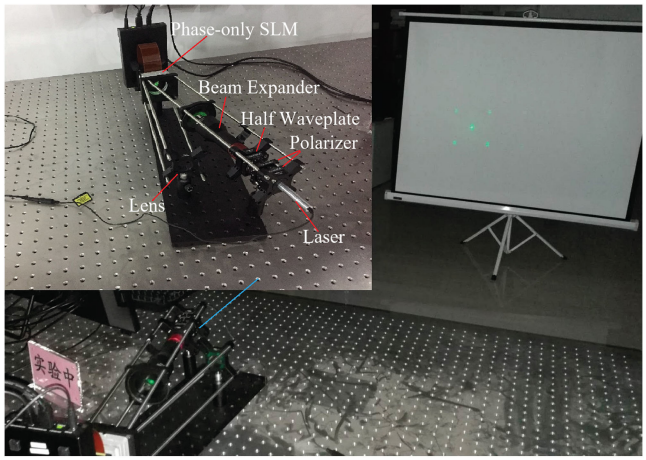

Fig. 6. Experimental setup and projected image at a longer distance.

liquid crystal material with high Δ always has a high viscosity, there is an optimized balance between d and Δ. The commercial products of highest response time for visible light is around several hundreds Hertz. To further improve the response time, special liquid crystal material should be utilized.

Next, we give an example to elaborate how to apply OMC to I2V scenario based on SLM. Consider the communication scenario in Fig. 1. We assume the optical source is attached on the road lamp which is 12 m high. The distance between two adjacent lamps is 50 m. Thus, the distance between the optical source and a car in a cell is in the range of 12$\sim$27.7 m (we only consider 2-dimension here). To ease the problem of tracking and reduce the hardware costs, non-coherent receiving is used here. A photo-diode (PD) is used to collect the optical power at the receiver side. The PD is attached on the top of a car. A beam is adapted to be directed to the PD. For stable communication, the beam coverage is set to be "wider" than the size of PD, as shown in Fig. 7. Assume the beam spot has an effective width of D which is larger than the size of PD denoted by d. Then, there will be a steady communication link during the procedure of PD moving from the left to the right of the beam spot. For example, if $D = 11$ cm, $d = 1$ cm and the speed of the car is $v = 60$ Km/h, the communication time is $t = (D - d)/v = 6$ ms,

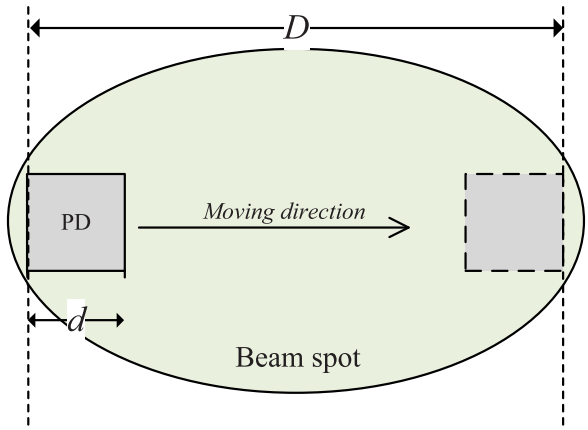

Fig. 7. Illustration of the position of PD and beam coverage.

corresponding to a refreshing frequency of 166.7 Hz, which is sufficient for hologram regeneration (see discussion in V). This approach makes the pointing and tracking task much easier in a moving scenario compared to coherent receiving schemes. PD array of larger receiving area can be used in the future to further improve the energy efficiency. A lens can also be attached on top of the PD to collect more power. This approach also reduces the difficulty of localization: centimeter level accuracy is needed and can be met by many available localization methods which will be discussed in Section V.

As for the optical efficiency, theoretically, there is no energy loss for pure phase SLM, since all incident light is reflected. However, there are still energy losses due to the absorption of liquid crystal and the reflection ratio of the top metal on the SLM. The total energy loss of the absorption of liquid crystal and top metal can be optimized to less than 10%. Another energy loss is due to the high order diffraction caused by the pixelating of the SLM. To reduce the energy of the high order replica, small pixel size is preferred. The optical energy loss indicates that

$$\sum_{n=1}^{N} |q_n|^2 < 1. \tag{11}$$

IV. Achievable Rate Analysis

As aforementioned, OMC is more attractive than FSO since the former aims to support multiple users simultaneously. In this section, we present theoretical analysis on the achievable rate region of OMC and the fundamental multi-user performance limit from information perspective for different multiple access schemes. The achievable rate is an upper bound of the throughput which is commonly used to evaluate the ultimate performance limit of different communication schemes. It is achieved only if many related factors are ideal or fit the signal model used in the rate analysis. Any non-ideal factor will result in a real throughput that is smaller than the achievable rate. Evaluating and minimizing the impact of various non-ideal factors falls into other important research topics and is out of the scope of this paper. In conventional OWC, the beams can not be adapted freely and the channels are fixed ones. For

example, the commonly used beam splitter can split a beam to two with a certain power ratio. However, that ratio will be fixed after the beam splitter is fabricated and cann't be tuned freely. Different from conventional OWC systems, OMC features that its multi-user channels q_n can be actively controlled through optical modules. We will show that this feature allows OMC to expand its achievable rate region significantly.

Without loss of generality, $N = 2$ users are assumed. The result can be easily extended to the cases of more users. The aggregate RF signal at the transmitter side is rewritten in discrete-time form:

$$u[n] = \sqrt{P_1}u_1[n] + \sqrt{P_2}u_2[n] \tag{12}$$

where $u_1[n]$ and $u_2[n]$ are the information signal intended for user-1 and user-2 at nth time slot, respectively. Here we assume $u_1[n]$ and $u_2[n]$ are i.i.d random variables with zero mean and unit variances. P_1 and P_2 are the allocated electrical powers for user-1 and user-2, respectively, which are subject to a total available power constraint $P_1 + P_2 \leq P$. At the receiver of user-i, the demodulated signal in electrical domain can be written as

$$\hat{u}_i[n] = q_i u[n] + w_i[n], i = 1, 2 \tag{13}$$

where q_i is the effective channel gain of user-i. Note that in the relatively short distance of an OMC cell, the propagation channel of a laser beam can be modeled as flat without fading and we can use q_i to describe *both* SLM power split and the propagation channel. Extension to a general model with attenuation is straightforward. In this regard, the effective channels will satisfy

$$|q_1|^2 + |q_2|^2 = \rho \tag{14}$$

where $\rho < 1$ represents possible power loss among the whole transmission process in practical systems. $w_i[n]$ is the additive white Gaussian noise (AWGN) of user-i which is zero mean and has full-band power of σ_n^2.

In general, a specific multiple access scheme will fall into only one of two categories of multiple access methods: orthogonal multiple access (OMA) and non-orthogonal multiple access (NOMA), depending on the correlations of the information signals $u_i[n]$, $i = 1, \ldots, N$, in all the resource domains. Take (12) as an example. For OMA schemes, $u_1[n]$ and $u_2[n]$ are uncorrelated in the given time and frequency grids, which can be realized by separating the two users in time or frequency domains. On the other hand, if $u_1[n]$ and $u_2[n]$ are correlated, e.g., user-1 and user-2 are distinguished only by their transmit powers, the scheme is referred to as NOMA. While NOMA can be viewed a generalization of OMA and thus intuitively more spectral efficient, OMA is usually simpler for system implementation. In this section, we derive the achievable rate region of OMC under the framework of both OMA and NOMA. The results are applicable to any specific multiple access scheme.

A. Orthogonal Multiple Access

In OMA, the available degree-of-freedom (DoF), either time or frequency, is split among the two users. Take frequency splitting as an example and assume the ratio of DoF allocated to user-1 as α. Then, at the receiver of user-1, by filtering the received signal to confine it into the allocated fraction of frequency band, the filtered signal of user-1 can be derived based on (12) and (13):

$$\tilde{u}_1[n] = q_1\sqrt{P_1}u_1[n] + \tilde{w}_1[n] \tag{15}$$

where $\tilde{u}_1[n]$ and $\tilde{w}_1[n]$ denote the filtered signal and noise of user-1, respectively. The collected power of interested signal is given by $|q_1|^2 P_1$. Since the normalized bandwidth of user-1 is reduced to α, the perceived power of the band-limited noise $\tilde{w}_1[n]$ reduces to $\alpha\sigma_n^2$ correspondingly. There is no multi-user interference in this scenario. User-2 has a similar received signal model with allocated DoF of ratio $(1 - \alpha)$. Therefore, we can write the achievable rates of the two users as

$$R_{1,oma} \leq R_o(\alpha, P_1, q_1, \sigma_n^2), \tag{16}$$

$$R_{2,oma} \leq R_o(1 - \alpha, P_2, q_2, \sigma_n^2), \tag{17}$$

where the units are bits/s/Hz and the function $R_o(\cdot)$ is defined by

$$R_o(\alpha, p, q, \sigma_n^2) = \alpha \log_2\left(1 + \frac{|q|^2 p}{\alpha\sigma_n^2}\right) \tag{18}$$

To obtain the boundary of the achievable rate region which includes all the feasible rate pairs of $(R_{1,oma}, R_{2,oma})$, realized by some combinations of P_1, P_2, q_1, q_2 and α, we transform the problem as an optimization problem (P1), which tries to find the maximal feasible value of $R_o(1 - \alpha, P_2, q_2, \sigma_n^2)$ for a given value of $R_o(\alpha, P_1, q_1, \sigma_n^2)$:

$$(\mathbf{P1}): \max_{\{P_2, q_2, \alpha\}} R_o(1 - \alpha, P_2, q_2, \sigma_n^2) \tag{19}$$

$$\text{s.t.} \quad \begin{cases} R_o(\alpha, P_1, q_1, \sigma_n^2) = r_1 \\ P_1 + P_2 \leq P \\ 0 \leq P_1 \leq P, 0 \leq P_2 \leq P \\ |q_1|^2 + |q_2|^2 = \rho \\ 0 \leq \alpha \leq 1 \end{cases} \tag{20}$$

where r_1 is a given value.

To solve (P1), the first constraint in (20) is transformed to $|q_1|^2 = g(\alpha)/P_1$, where $g(\alpha) = \alpha(2^{r_1/\alpha} - 1)\sigma_n^2$. Notice that $R_o(1 - \alpha, P_2, q_2, \sigma_n^2)$ is an increasing function of P_2 and $P_2 \leq P - P_1$, the objective function of (P1) can be transformed to

$$\begin{aligned} &R_o(1 - \alpha, P - P_1, q_2, \sigma_n^2) \\ &\quad = (1 - \alpha)\log_2\left(1 + \frac{(P - P_1)(\rho - \frac{g(\alpha)}{P_1})}{(1 - \alpha)\sigma_n^2}\right) \\ &\quad = (1 - \alpha)\log_2\left(1 + \frac{P\rho + g(\alpha) - (P_1\rho + \frac{Pg(\alpha)}{P_1})}{(1 - \alpha)\sigma_n^2}\right) \end{aligned} \tag{21}$$

which is a *concave* function of P_1. For a given α, $R_o(1 - \alpha, P - P_1, q_2, \sigma_n^2)$ achieves its maximum value at $P_1^* = \sqrt{\frac{Pg(\alpha)}{\rho}}$. Note that $|q_2|^2 = \rho - g(\alpha)/P_1 \geq 0$ guarantees $P_1^* \leq P$ and $|q_1|^2 =$

$g(\alpha)/P_1 \geq 0$ guarantees $P_1^* \geq 0$. Thus, the original problem reduces to a simple single variable (of α) optimization problem which can be efficiently solved by gradient or line search approaches.

By varying r_1 from 0 to its maximum value, which is $\log_2\left(1+\rho P/\sigma_n^2\right)$ by allocating all power ($P_1 = P, |q_1|^2 = \rho$) and DoF to it, we will finally obtain the entire boundary of the feasible rate region of OMA-based OMC.

B. Non-Orthogonal Multiple Access

In NOMA, the available DoF is fully utilized by all users simultaneously thus it allows for superposition of the users' signals. Based on (12) and (13), we can write the received signal models of user-1 and user-2 in NOMA as

$$\hat{u}_1[n] = q_1\sqrt{P_1}u_1[n] + q_1\sqrt{P_2}u_2[n] + w_1[n] \tag{22}$$

$$\hat{u}_2[n] = q_2\sqrt{P_1}u_1[n] + q_2\sqrt{P_2}u_2[n] + w_2[n] \tag{23}$$

Since the powers of $w_1[n]$ and $w_2[n]$ are assumed to be the same, when $|q_1| < |q_2|$ such that user-2 has better channel quality, we can safely claim that in an average sense, as long as user-1 can successfully decode its data $u_1[n]$ from $\hat{u}_1[n]$, then user-2, which has higher signal-to-noise ratio (SNR) of $u_1[n]$, should also be able to decode $u_1[n]$ from $\hat{u}_2[n]$. However, it can not be guaranteed that user-1 can decode any symbol that user-2 can successfully decode. As a consequence, when the receiver of user-1 tries to decode its data $u_1[n]$, the signal of user-2 has to be treated as background interference which is independent of the signal of user-1 and contributes a power of $|q_1|^2P_2$. Therefore, the achievable rate of user-1 is limited by

$$R_{1,noma} \leq \log_2\left(1+\gamma_1(|q_1|)\right) \tag{24}$$

where the function $\gamma_1(x)$ denotes the SNR of user-1 and is defined by

$$\gamma_1(x) = \frac{x^2P_1}{x^2P_2+\sigma_n^2} \tag{25}$$

On the other hand, at the receiver of user-2, the SNR of symbol $u_1[n]$ becomes $\gamma_1(|q_2|)$ which is larger than $\gamma_1(|q_1|)$ since $\gamma_1(x)$ is a monotonic increasing function. In this case, user-2 can successfully decode $u_1[n]$ with a larger SNR than that at user-1's receiver. Therefore, as long as the rate of $u_1[n]$ is confined by $\log_2\left(1+\gamma_1(|q_1|)\right)$, user-2 is capable of perfectly decode and remove user-1's signal from $\hat{u}_2[n]$ and the remaining signal becomes

$$\tilde{u}_2[n] = q_2\sqrt{P_2}u_2[n] + w_2[n] \tag{26}$$

which is interference-free. Now the achievable rate of user-2 is given by

$$R_{2,noma} \leq \log_2\left(1+\frac{|q_2|^2P_2}{\sigma_n^2}\right) \tag{27}$$

Similarly, when $|q_1| \geq |q_2|$, we obtain the achievable rate pair of user-1 and user-2 in NOMA-based OMC as

$$R_{1,noma} \leq \log_2\left(1+\frac{|q_1|^2P_1}{\sigma_n^2}\right) \tag{28}$$

$$R_{2,noma} \leq \log_2\left(1+\frac{|q_2|^2P_2}{|q_2|^2P_1+\sigma_n^2}\right) \tag{29}$$

To obtain the boundary of the achievable rate region which includes all the feasible rate pairs of $(R_{1,noma}, R_{2,noma})$ with different power allocation and split ratios among P_1, P_2 and q_1, q_2, we can transform the problem to a pair of optimization problems:

$$(\mathbf{P2-A}): \max_{\{P_2,q_2\}} \log_2\left(1+\frac{|q_2|^2P_2}{\sigma_n^2}\right) \tag{30}$$

$$\text{s.t.} \quad \begin{cases} \log_2\left(1+\frac{|q_1|^2P_1}{|q_1|^2P_2+\sigma_n^2}\right) = r_1 \\ P_1+P_2 \leq P \\ 0 \leq P_1 \leq P, 0 \leq P_2 \leq P \\ |q_1|^2+|q_2|^2 = \rho \\ |q_1| \leq |q_2| \end{cases} \tag{31}$$

$$(\mathbf{P2-B}): \max_{\{P_2,q_2\}} \log_2\left(1+\frac{|q_2|^2P_2}{|q_2|^2P_1+\sigma_n^2}\right) \tag{32}$$

$$\text{s.t.} \quad \begin{cases} \log_2\left(1+\frac{|q_1|^2P_1}{\sigma_n^2}\right) = r_1 \\ P_1+P_2 \leq P \\ 0 \leq P_1 \leq P, 0 \leq P_2 \leq P \\ |q_1|^2+|q_2|^2 = \rho \\ |q_1| \geq |q_2| \end{cases} \tag{33}$$

where r_1 is a given value. Mathematically, (P2-A) and (P2-B) are even simpler than (P1) and can be efficiently solved. Without going into details of the derivation, we give the results of (P2-A) and (P2-B) in the following. For (P2-A), the maximum value of the objective function is given by

$$R_{2,a}^* = R_{opt}(r_1) \tag{34}$$

The function $R_{opt}(r)$ is defined as

$$R_{opt}(r) = \log_2\left(1+\frac{\rho p(r)}{\sigma_n^2} - \frac{2^r-1}{\frac{P}{p(r)}-2^r}\right) \tag{35}$$

where the function $p(r)$ represents the optimal value of the allocated power P_2 for user-2 and is defined by

$$p(r) = \frac{P - \max\left\{\sqrt{\frac{\sigma_n^2P(2^r-1)}{\rho}}, \frac{2\sigma_n^2(2^r-1)}{\rho}\right\}}{2^r} \tag{36}$$

By varying the feasible value of r_1 in (P2-A) from 0 to its maximum value which is $\log_2\left(1+\rho P/(2\sigma_n^2)\right)$ when $P_1 = P$ and $|q_1|^2 = \rho/2$ ($|q_1|^2 \leq \rho/2$ in (P2-A)), we can get the boundary curve obtained by solving (P2-A). To solve (P2-B), while the similar approach could be applied as in (P2-A) (the result

is somewhat more complex), there is a better way by exploiting the duality of the two problems:

Proposition 1: if $(r_{1,a}, R^*_{2,a})$ lies on the boundary of the achievable rate region deduced from (P2-A), then $(r_{1,b} = R^*_{2,a}, R^*_{2,b} = r_{1,a})$ lies on the boundary of the achievable rate region deduced from (P2-B).

Proof: The job of (P2-B) can be reformulated as finding the maximum rate of user-1 for a given rate of user-2. By changing the given rate of user-2 from 0 to its maximum value, which is also $\log_2\left(1+\rho P/(2\sigma_n^2)\right)$ when $|q_2|^2 = \rho/2$ and $P_2 = P$), the boundary of the achievable rate region in the case of $|q_1| \geq |q_2|$ will be obtained, which has to be the same as will be obtained by solving the original problem (P2-B). However, this new optimization problem has exactly the same formulation as (P2-A) if we redefine user-1 as user-2 and redefine user-2 as user-1. As a consequence, Proposition 1 holds.

Finally, the desirable boundary of the rate region of NOMA is the envelop of the two boundary curves obtained by (P2-A) and (P2-B).

Remarks: Based on Proposition 1, we can predict that: i) the achievable rate region of NOMA based OMC is symmetric with respect to the line $R_1 = R_2$. In fact, OMA also entitles this feature as a result of controllable channel in OMC. ii) The rate region is expanded as compared to any fixed pair of (q_1, q_2), which means OMC has larger rate region compared to conventional schemes in which the effective channels q_1 and q_2 are fixed. In particular, the maximum rate of both users in OMC are expanded to $\log_2\left(1+\rho P/\sigma_n^2\right)$ (set $r_1 = 0$ and $|q_2|^2 = \rho$ in (P2-A)), which could be much larger than the case with fixed channel coefficients, especially for users with small channel gains. iii) As a consequence of (ii), the sum rate performance with maximally user fairness, will also be improved. With symmetric rate region, the maximally user fairness is achieved when $R_1 = R_2$ on the boundary of the rate region. It wouldn't be hard to derive that in this case, the sum rate of OMA and NOMA are given by

$$R_{sum,oma} = \log_2\left(1+\frac{\rho P}{2\sigma_n^2}\right) \tag{37}$$

$$R_{sum,noma} = 2R_{opt}(r^*) \tag{38}$$

where r^* satisfy

$$R_{opt}(r^*) = r^* \tag{39}$$

Those features allows OMC to allocate the resources to users with improved balance of performance and user fairness.

C. Numerical Examples

In this subsection, we present some numerical examples to show the behaviour of the rate regions of OMA and NOMA in OMC. We will compare OMC to conventional OWC schemes in which the channel gains are fixed and can not be actively tuned. To do so, we fix the total transmit SNR, defined by $10\log_{10}\frac{P}{\sigma_n^2}$, to be 20 dB. The power loss factor is set to be $\rho = 0.8$. For fixed channel gains, we test two cases: for the first configuration ('Config-1' in the legend), we assume $|q_1|^2 = 0.1$. Correspondingly, $|q_2|^2 = \rho - |q_1|^2 = 0.7$. For the second configuration ('Config-2' in the legend), we set $|q_1|^2 = 0.6$ and $|q_2|^2 = 0.2$ to deviate largely from the first configuration. Fig. 8 plots the rate regions of OMC and conventional schemes (denoted as 'fixed channel' in the legend) using OMA and NOMA, respectively. Several facts could be observed from Fig. 8. Firstly, NOMA has larger rate region than its OMA counterpart for both fixed channels and adjustable channels. For conventional OWC, the specific channels have great impacts on the rate region: for any given pair of fixed channels, only a portion of the rate region of OMC could be achieved, which can not be well adapted to various channel conditions. Secondly, with adjustable channels in OMC, the rate regions of both NOMA and OMA are enlarged compared to the case of fixed channels and each user can achieve a higher single-user rate. This is inline with the predictions in previous subsection. Thirdly, it is seen that in OMC, the gap between OMA and NOMA is not as large as that in the case of fixed channels. To elaborate, Fig. 9 plots the sum rate gap between OMA and NOMA based OMC with respect to different SNR values. Here, the sum rate is chosen to guarantee maximum user fairness, i.e., it is calculated with the symmetric rate constraint $R_1 = R_2$ (c.f. (37) and (38)) for both OMA and NOMA[2]. It can be seen that the gap approaches to a constant (1 bits/s/Hz in this configuration) at high SNR range. In other words, in OMC with controllable channels, we can use low-cost OMA schemes while collecting a large portion of potential gains provided by using more complicated NOMA schemes, which is a desired feature from implementation perspective.

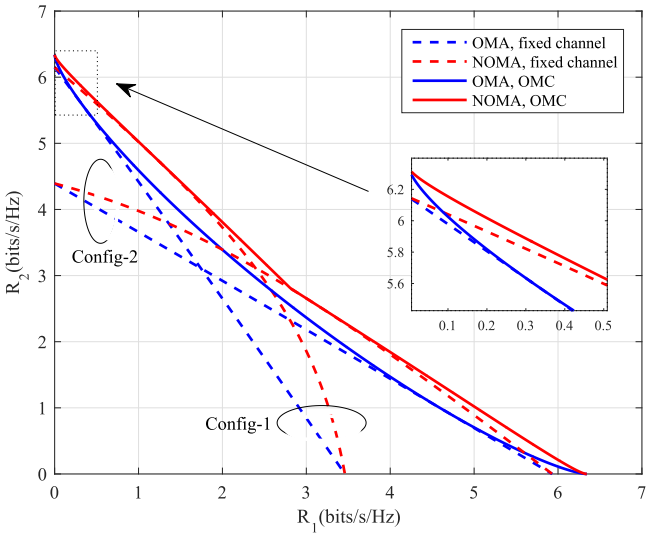

Fig. 8. The achievable rate regions of OMC using OMA and NOMA schemes with and without channel controlling.

V. Discussions

A. Localization Methods

One of the key technical issues for the functionality of OMC is the acquisition of the accurate spatial positions of mobile terminals. Wireless localization could be realized through radio

[2]It is found in Fig. 8 that this sum rate is the smallest but the most fair one on the boundary.

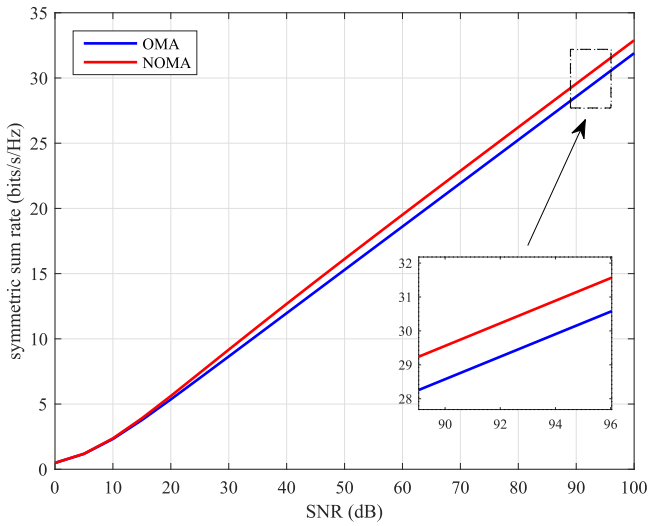

Fig. 9. Symmetric sum rate comparison of OMA and NOMA with adjustable channels.

signals, optical signals, inertial navigation, image recognition, and other viable methods. For example, centimeter-level precision could be achieved using ultra-wideband signal for localization [29]. Even higher precision is possible if multi-point localization anchors or larger bandwidth are involved. A promising localization method for OMC is target tracking based on image recognition [30]. At the transmitter side, a high speed camera is used to capture the image of the communication area. The receivers are set as the targets in the image. Then image recognition is applied to distinguish the targets from the observed image and adjust the SLM to focus laser beams properly. As PD is attached on a big car, a coarse-fine recognition step can be employed. This localization method does not require the targets to emit radio or optical signals and thus eliminates the feedback links. In addition, image processing and recognition is already a mature technology. In the real-time tracking with high speed camera, the delay time (including the time of image acquisition and processing) can be reduced to milliseconds [31], [32]. To generate the hologram, we only need to perform inverse FRFT of the image itself after setting the receiver locations "bright" and other locations "dark". Since the image is "sparse", very efficient transform algorithms (see for example [33]) can be used for fast generation of the hologram. In addition, as the cars are moving steadily, receiver locations on successive images do not change suddenly and can be predicted with high accuracy, which can be further exploited to accelerate the hologram generation. Finally, if dedicated integrated circuit is used in real application, the calculation can be much faster than software based calculation. Therefore, target tracking based on image recognition is a suitable and feasible localization method for OMC.

B. Background Radiation

Background radiation due to solar irradiance is an important issue in practical FSO design [34], [35]. Therefore, it is equally important in OMC as OMC also involves the radiation from the lamps at night. If not handled properly, the PD may get saturated with undesirable light interference. Fortunately, it has been recognized in literature that the chance of collecting direct sunlight is low and also predictable [35]. Several approaches are available and commonly employed which can well tackle this problem. The most widely used approach is to use a narrow spectral bandpass filter and a spatial filter, prior to photo-detection [36], [37]. This step will filter out most portion of the background radiation. Above on this, another means to avoid the saturation problem is to utilize high-saturation-current photodiode [38], [39]. In general, with deliberate design, the saturation current of a photodiode can be orders higher than that caused by direct sunlight and direct lamp light, thus avoiding saturation. For example, in [38], the saturation current corresponds to a received power up to 36 KW/cm^2. This is way higher than the average annual solar radiation arriving at the *top* of the Earth's atmosphere which is roughly 1.36 KW/m^2 [40]. 36 KW is also way higher than the *total* radiated power of a usual street lamp. Other available approaches to tackle saturation includes using lasers with specific wavelength and by signaling design [41].

C. Signal Power Fluctuations Within the Beam/Cell

Due to some non-ideal factors in the system, there will be potential fading effect represented by signal power fluctuations within a beam spot and we have to take measures to alleviate its extent. Firstly, by carefully setting the control signal $f(v_1, v_2)$, we can generate a desired beam spot without sudden signal power fluctuations, especially when considering the power integral effect of the PD. Secondly, with a beam expander, we can project the expanded laser beam onto the SLM such that the beam power distribution is approximately uniform on the surface of the SLM. Finally, to avoid any outage due to the transition state at the edge of the beam spot, we can generate a longer beam and restrict the PD into the center part of the beam. With those means, the fluctuation of the received signal power within a beam spot can be restrained to a low level.

Another form of signal power fluctuation exhibits as the receiver moves toward or away from a lamp, which is closely related to the cell coverage and handover. With fixed receiving angle of the PD, the received power can fluctuate in a wide range. In such a case, tradeoffs should be done. For example, the transmitter can allocate more power to the user when it is at the edge of a cell to improve its performance. The power budget of the optical source can be chosen such that the worst-case performance is guaranteed at the cell edge. In this regard, the cell coverage is still mainly determined by the infrastructure. Alternatively, one can deploy ATP system as well as array of PDs with diverse receiving angles to maintain a relatively stable power within the cell coverage. The optical sources can be connected by wire or wireless techniques to facilitate coordination and handover. Handover is a common issue in cellular communications. However, OMC has its unique feature compared with RF communication. In RF communication, the handover appears to be opportunistic because of the randomness of the communication channels between the user and different base stations. The time/location/base-station-to-choose are highly random at

the cell edges. In contrast, OMC represents a relatively *static* scenario: the location and cell to handover are highly fixed, and the time for handover is highly predictable. Therefore, handover in OMC is expected to be easier than that in RF.

D. OPA Implementation

In previous sections, we used SLM for beam adaptation. There are other possible ways to implement OPA such as nanophotonic phased array (NPA) [42] and digital micromirror device (DMD) [43]. NPA is similar to its RF counterpart, consisting of many typically identical optical antennas. Each antenna emits light of a particular amplitude and phase. By interfering with these emissions, a desired far field radiation pattern is formed. MIT has designed a large-scale, compact NPA system that is compatible with complementary metal-oxide-semiconductor (CMOS) processers, including 64×64 optical nano-antennas on silicon wafers [44]. All 4096 optical nanostructures are balanced in power to produce a complex radiation pattern. Since the wavelength is much shorter than RF, NPA potentially supports excessive number of antenna elements to generate arbitrary radiation patterns. It is expected that the future development of NPA will make the beam track more accurate. Another OPA implementation form is laser beam deflection based on DMD. At present, DMD chip is mature and highly reliable [45]. At the same time, it entitles high frequency of flip and short response time ($2\sim5\ \mu$s) [46], [47], which renders very fast controlling. The drawback is that most of the current DMD can only be locked at two predefined angles [48], [49], which can not be accurately deflected to angles in the middle. Thus, only coarse beam adaptation can be achieved using current DMD. Calibration with other technologies is needed to get finer adaptation. More advanced DMD with finer adjustable lock angles is desired in OMC.

E. New Problems in Signal Processing

Due to the unique feature of OMC, i.e., the effective per user channel is controllable, it will bring many new problems and research opportunities in signal processing. One open issue is the performance analysis for the case of multiple SLM simultaneously serving users. Section IV only investigates the achievable rate of NOMA and OMA with single SLM and photodetector. The capacity of such a channel model and the gap between the achievable rate and channel capacity are fundamental performance limits and remain unknown. Extended capacity and rate analysis for the case of multiple SLM and photodetectors is non-trivial and quite difficult due to the new dimension of degree-of-freedom. It is expected that OMC outperforms legacy systems with large gains as indicated by Section IV. Nonetheless, to claim the potential gain, effective and efficient resource scheduling algorithms are mandatary. For example, how to efficiently utilize resources in time, spatial, power, frequency, polarization, and orbital angular momentum domains in the new scenario of OMC, are required, which leads to new challenging optimization problems. Besides resource scheduling, other signal processing problems such as channel estimation and feedback, high order components elimination of SLM, as well as cell-switching, are to be solved for efficient functionality of OMC.

VI. Conclusion

This paper proposed a new communication technology called OMC which utilizes laser-beam-based optical communication to simultaneously serve multiple high-mobility users with ultra-high throughput. It is a natural evolution of current RF communication to future communication schemes which require high data rate multi-user mobile communication using high frequency spectrum. It also provides a possibility of supporting QKD in future quantum communications. The paper discussed the system model and the implementation form of OMC using SLM as a means to split and concentrate energy to desired users. It is shown that the channel has a new feature compared with the system with antennas emitting RF signal, i.e., the effective channel is controllable. This feature makes the OMC potentially outperform the legacy systems with fixed channel gains, which is proved by rate region analysis. Finally, feasibility and challenges in signal processing are discussed for future research of OMC.

Acknowledgment

The authors would like to thank the anonymous reviewers for their valuable suggestions to improve their work.

References

[1] R. A. DiFazio and P. J. Pietraski, "The bandwidth crunch: Can wireless technology meet the skyrocketing demand for mobile data?" in *Proc. IEEE Long Island Syst., Appl. Technol. Conf.*, Farmingdale, NY, USA, May 6, 2011, pp. 1–6.

[2] J. G. Andrews, S. Singh, Q. Ye, X. Lin, and H. S. Dhillon, "An overview of load balancing in HetNets: Old myths and open problems," *IEEE Wireless Commun.*, vol. 21, no. 2, pp. 18–25, Apr. 2014.

[3] D. C. Sicker and L. Blumensaadt, "The wireless spectrum crunch: White spaces for 5G?" in *Fundamentals of 5G Mobile Networks*. Hoboken, NJ, USA: Wiley, 2015, ch. 7, pp. 165–189.

[4] J. Zander, "Beyond the ultra-dense barrier: Paradigm shifts on the road beyond 1000x wireless capacity," *IEEE Wireless Commun.*, vol. 24, no. 3, pp. 96–102, Jun. 2017.

[5] M. Kavehrad, "Optical wireless applications—A solution to ease the wireless airwaves spectrum crunch," in *Proc. SPIE 8645, Broadband Access Commun. Technol. VII*, Art. no. 86450G, Feb. 2013.

[6] M. Kavehrad, "MEMS-based reconfigurable optical wireless networking in data centers," in *Proc. IEEE Photon. Conf.*, Orlando, FL, USA, Oct. 1–5, 2017, pp. 127–128.

[7] T. L. Marzetta, "Noncooperative cellular wireless with unlimited numbers of base station antennas," *IEEE Trans. Wireless Commun.*, vol. 9, no. 11, pp. 3590–3600, Nov. 2010.

[8] J. Hoydis, S. Ten Brink, and M. Debbah, "Massive MIMO in the UL/DL of cellular networks: How many antennas do we need?," *IEEE J. Sel. Areas Commun.*, vol. 31, no. 2, pp. 160–171, Feb. 2013.

[9] L. Lu, G. Y. Li, A. L. Swindlehurst, A. Ashikhmin, and R. Zhang, "An overview of massive MIMO: Benefits and challenges," *IEEE J. Sel. Topics Signal Process.*, vol. 8, no. 5, pp. 742–758, Oct. 2014.

[10] E. Björnson, E. G. Larsson, and T. L. Marzetta, "Massive MIMO: Ten myths and one critical question," *IEEE Commun. Mag.*, vol. 54, no. 2, pp. 114–123, Feb. 2016.

[11] T. Komine and M. Nakagawa, "Fundamental analysis for visible-light communication system using LED lights," *IEEE Trans. Consum. Electron.*, vol. 50, no. 1, pp. 100–107, Feb. 2004.

[12] H. Hass, L. Yin, Y. Wang, and C. Chen, "What is LiFi?" *IEEE J. Lightw. Technol.*, vol. 34, no. 6, pp. 1533–1544, Mar. 2016.

[13] M. A. Khalighi and M. Uysal, "Survey on free space optical communication: A communication theory perspective," *IEEE Commun. Surv. Tut.*, vol. 16, no. 4, pp. 2231–2258, Nov. 2014.
[14] T. Nguyen, K. Riesing, R. Kingsbury, and K. Cahoy, "Development of a pointing, acquisition, and tracking system for a CubeSat optical communication module," in *Proc. SPIE, Free-Space Laser Commun. Atmos. Propag. XXVII*, Mar. 2015, vol. 9354, pp. 93540O-1–93540O-9.
[15] Z. Zhang, L. Wu, J. Dang, G. Zhu, J. Hu, H. Jiang, and X. You, "Optical mobile communications: Principles and challenges," in *Proc. Wireless Opt. Commun. Conf.*, Newark, NJ, USA, Apr. 7-8, 2017, pp. 1–4.
[16] V. Scarani, H. B.-Pasquinucci, N. J. Cerf, M. Dušek, N. Lütkenhaus, and M. Peev, "The security of practical quantum key distribution," *Rev. Mod. Phys.*, vol. 81, no. 3, pp. 1301–1350, Sep. 2009.
[17] X. Wang *et al.*, "Millimeter wave communication: A comprehensive survey," *IEEE Commun. Surv. Tut.*, vol. 20, no. 3, pp. 1616–1653, Jul.–Sep. 2018.
[18] P. F. Mcmanamon *et al.*, "Optical phased array technology," *Proc. IEEE*, vol. 84, no. 2, pp. 268–298, Feb. 1996.
[19] L. Ge, M. Duelli, and R. Cohn, "Enumeration of illumination and scanning modes from real-time spatial light modulators," *Opt. Express*, vol. 7, no. 12, pp. 403–416, Dec. 2000.
[20] D. Wang, B. Jin, Y. Wang, and P. Jia, "Adaptive flattop beam shaping with a spatial light modulator controlled by the holographic tandem method," *IEEE Photon. J.*, vol. 8, no. 1, pp. 1–7, Feb. 2016.
[21] M. Sutkowski and M. Kujawinska, "Application of liquid crystal (LC) devices for optoelectronic reconstruction of digitally stored holograms," *Opt. Lasers Eng.*, vol. 33, no. 3, pp. 191–201, Mar. 2000.
[22] N. Mukohzaka, N. Yoshida, H. Toyoda, Y. Kobayashi, and T. Hara, "Diffraction efficiency analysis of a parallel-aligned nematic-liquid-crystal spatial light modulator," *Appl. Opt.*, vol. 33, no. 14, pp. 2804–2811, May 1994.
[23] V. Namias, "The fractional order Fourier transform and its application to quantum mechanics," *IMA J. Appl. Math.*, vol. 25, no. 3, pp. 241–265, Mar. 1980.
[24] A W. Lohmann, "Image rotation, Wigner rotation, and the fractional Fourier transform," *J. Opt. Soc. Amer. A*, vol. 10, no. 10, pp. 2181–2186, Oct. 1993.
[25] D. Mendlovic and H. M. Ozaktas, "Fractional Fourier transforms and their optical implementation: I," *J. Opt. Soc. Amer. A*, vol. 10, no. 9, pp. 1875–1881, Sep. 1993.
[26] H. M. Ozaktas and D. Mendlovic, "Fractional Fourier transforms and their optical implementation: II," *J. Opt. Soc. Amer. A*, vol. 10, no. 12, pp. 2522–2531, Dec. 1993.
[27] J. Hua, L. Liu, and G. Li, "Extended fractional Fourier transforms," *J. Opt. Soc. Amer. A*, vol. 14, no. 12, pp. 3316–3322, Dec. 1997.
[28] W. Jin, C. Yan, L. Ma, H. Ye, and H. Wang, "Joint extended fractional Fourier transform correlator," *Opt. Commun.*, vol. 268, no. 1, pp. 34–37, Dec. 2006.
[29] R. Ye, S. Redfield, and H. Liu, "High-precision indoor UWB localization: Technical challenges and method," in *Proc. IEEE Int. Conf. Ultra-Wideband*, Nanjing, China, Sep. 20–23, 2010, pp. 1–4.
[30] D. Wang, H. Lu, and M. H. Yang, "Online object tracking with sparse prototypes," *IEEE Trans. Image Process.*, vol. 22, no. 1, pp. 314–325, Jan. 2013.
[31] W. Luo *et al.*, "Multiple object tracking: A literature review," unpublished paper, 2017. [Online]. Available: https://arxiv.org/abs/1409.7618
[32] T. Nawaz, F. Poiesi, and A. Cavallaro, "Measures of effective video tracking," *IEEE Trans. Image Process.*, vol. 23, no. 1, pp. 378–388, Jan. 2014.
[33] A. Agarwal, H. Hassanieh, O. Abari, E. Hamed, D. Katabi, and Arvind, "High-throughput implementation of a million-point sparse Fourier transform," in *Proc. Int. Conf. Field Programmable Logic Appl.*, Munich, Germany, Sep. 2–4, 2014, pp. 1–6.
[34] W. R. Leeb, "Degradation of signal to noise ratio in optical free space data links due to background illumination," *Appl. Opt.*, vol. 28, no. 15, pp. 3443–3449, Aug. 1989.
[35] V. G. Sidorovich, "Solar background effects in wireless optical communications," in *Proc. SPIE, Opt. Wireless Commun. V*, Dec. 2002, vol. 4873, pp. 133–142.
[36] A. K. Majumdar and J. C. Ricklin. *Free-Space Laser Communications: Principles and Advances*. New York, NY, USA: Springer-Verlag, 2008, sec. 2.3.7.
[37] M. A. Khalighi and M. Uysal, "Survey on free space optical communication: A communication theory perspective," *IEEE Commun. Surv. Tut.*, vol. 16, no. 4, pp. 2231–2258, Oct.–Dec. 2014.
[38] Z. Li, H. Pan, H. Chen, A. Beling, and J. C. Campbell, "High-saturation-current modified uni-traveling-carrier photodiode with cliff layer," *IEEE J. Quantum Electron.*, vol. 46, no. 5, pp. 626–632, May 2010.
[39] T. Shi, B. Xiong, C. Sun, and Y. Luo, "Back-to-back UTC-PDs with high responsivity, high saturation current and wide bandwidth," *IEEE Photon. Technol. Lett.*, vol. 25, no. 2, pp. 136–139, Jan. 2013.
[40] O. Coddington, J. L. Lean, P. Pilewskie, M. Snow, and D. Lindholm, "A solar irradiance climate data record," *Amer. Meteorol. Soc.*, vol. 97, no. 7, pp. 1265–1282, Jul. 2016.
[41] M. A. Khalighi, F. Xu, Y. Jaafar, and S. Bourennane, "Double-laser differential signaling for reducing the effect of background radiation in free-space optical systems," *IEEE/OSA J. Opt. Commun. Netw.*, vol. 3, no. 2, pp. 145–154, Feb. 2011.
[42] C. V. Poulton *et al.*, "Large-scale silicon nitride nanophotonic phased arrays at infrared and visible wavelengths," *Opt. Lett.*, vol. 42, no. 1, pp. 21–24, Jan. 2017.
[43] P. Karkamkar and R. Gutierrez-Osuna, "Optical computation of chemometrics projections using a digital micromirror device," in *Proc. IEEE Int. Symp. Olfaction Electron. Nose*, Montreal, QC, Canada, May 28–31, 2017, pp. 1–3.
[44] J. Sun, E. Timurdogan, A. Yaacobi, E. S. Hosseini, and M. R. Watts, "Large-scale nanophotonic phased array," *Nature*, vol. 493, no. 7431, pp. 195–199, Jan. 2013.
[45] H. F. Taylor and J. C. Juarez, "Field test of a distributed fiber-optic intrusion sensor system for long perimeters," *Appl. Opt.*, vol. 46, no. 11, pp. 1968–1971, Apr. 2007.
[46] A. D. Kersey, "Distributed and multiplexed fiber optic sensors," in *Fiber Optic Sensors: An Introduction for Engineers and Scientists*, 2nd ed. Hoboken, NJ, USA: Wiley, Jul. 2011, pp. 277–314.
[47] J. P. Dakin, D. A. J. Pearce, A. P. Strong, and C. A. Wade, "A novel distributed optical fibre sensing system enabling location of disturbances in a Sagnac loop interferometer," in *Proc. SPIE 0838, Fiber Opt. Laser Sensors V*, Mar. 1988, pp. 325–328.
[48] L. J. Hornbeck, "Digital light processing™: A new MEMS-based display technology," *Tech. Dig. IEEJ 14th Sensor Symp.*, Kawasaki, Japan, Jun. 4–5, 1996, pp. 297–304.
[49] S. A. Goorden, J. Bertolotti, and H. Yilmaz, "High-resolution phase and amplitude modulation using a digital micromirror device," in *Proc. IEEE Eur. Conf. Lasers Electro-Opt. Int. Quantum Electron. Conf.*, Munich, Germany, May 12–16, 2013, p. 1.

Zaichen Zhang (SM'15) received the B.S. and M.S. degrees in electrical and information engineering from Southeast University, Nanjing, China, in 1996 and 1999, respectively, and the Ph.D. degree in electrical and electronic engineering from the University of Hong Kong, Hong Kong, in 2002. From 2002 to 2004, he was a Postdoctoral Fellow with the National Mobile Communications Research Laboratory, Southeast University. He is currently a Professor with Southeast University. He has authored more than 200 papers and issued 30 patents. His current research interests include 6G mobile information systems, optical wireless communications, and quantum information technologies.

Jian Dang (M'15) received the B.S. degree in information engineering in July 2007 and Ph.D. degree in information and communications engineering in September 2013, both from Southeast University, Nanjing, China. From September 2010 to March 2012, he was a Visiting Scholar with the Department of Electrical and Computer Engineering, University of Florida, Gainesville, FL, USA. Since September 2013, he has been with the National Mobile Communications Research Laboratory, Southeast University, Nanjing, China, first as a Lecturer and as an Associate Professor from 2017. His research interests include signal processing in wireless communications, non-orthogonal multiple access schemes, and optical wireless communications.

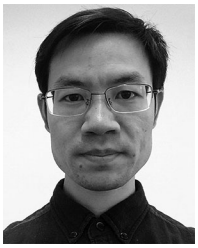

Liang Wu (M'13) received the B.S. degree in 2007, the M.S. degree in 2010, and the Ph.D. degree in 2013, all from School of Information Science and Engineering, Southeast University, Nanjing, China. From September 2011 to March 2013, he was a Visiting Student with the School of Electrical Engineering and Computer Science, Oregon State University. He is currently an Associate Professor with the National Mobile Communications Research Laboratory, Southeast University, Nanjing, China. His research interests include indoor optical wireless communications, multiple-input and multiple-output wireless communication systems, and interference alignment.

Haibo Wang (M'18) received the B.S. degree in information engineering from School of Information Science and Engineering, Southeast University, Nanjing, China, in 2018. He is currently working toward the master's degree in communication engineering at Southeast University. His research interests include mainly optical beam scanning technology in optical mobile communication, and application of optical phased array.

Jun Xia received the B.S. degree from the College of Automation Engineering, Nanjing University of Aeronautics and Astronautics, Nanjing, China, in 1996, and the M.S. and Ph.D. degrees from School of Electronic Science and Engineering, Southeast University, Nanjing, China, in 1999 and 2004, respectively. Supported by Program of the Ministry of Education of China for introducing Talents of Discipline to Universities, he visited the Delft University of Technology as a Visiting Professor in 2007. He is currently a Professor with Joint International Research Laboratory of Information Display and Visualization, Southeast University. His research interests include the autostereoscopic display, holographic display, and flexible display. He has the charge of several national high technology programs focusing on three-dimensional display and the phase-only spatial light modulator devices. He has authored or coauthored more than 100 scientific papers and has more than 60 patents.

Wei Lei is a Professor with the Department of Electronic Engineering, Southeast University, Nanjing, China. His first research activities were focused on charged particle optics and application in display devices. He received his Ph.D. degree from Southeast University, in 1993. Since 1994, he was involved in project cooperation between Southeast University and Philips Company. He has designed a few new electron guns for cathode ray tubes, and he also investigated the method to improve the sensitivity of deflection coil. Since 1995, he has finished 22 collaborative projects between university and industries. Now, his research fields cover the nano-materials for photonic detectors, field-effect transistor based on nano-wires, 3-D display technologies, and micro-displays. He has authored or coauthored more than 150 papers in scientific journals, issued 28 patents, and given more than 30 invited speeches and oral presentations in conferences.

Jiangzhou Wang (F'17) is currently a Professor and the former Head with the School of Engineering and Digital Arts, University of Kent, Canterbury, U.K. He has authored three books, and more than 250 papers in international journals and conferences in the area of wireless mobile communications. His research interests include distributed antenna systems and C-RAN, NOMA, massive MIMO and beamforming, D2D and vehicular communications, and emergency communications. He is the resipient of the Best Paper Award from the IEEE GLOBECOM2012 and was an IEEE Distinguished Lecturer from 2013 to 2014. He was an Editor for a number of international journals including the IEEE TRANSACTIONS ON COMMUNICATIONS from 1998 to 2013. He is the Technical Program Chair of the IEEE ICC2019, Shanghai. He was the Executive Chair of the IEEE ICC2015, London, U.K., and the TPC Chair of the IEEE WCNC2013. He is a Fellow of the Royal Academy of Engineering (U.K.), and Fellow of IET.

Xiaohu You (F'12) received the B.S., M.S., and Ph.D. degrees in electrical engineering from the Nanjing Institute of Technology, Nanjing, China, in 1982, 1985, and 1989, respectively. From 1987 to 1989, he was a Lecturer with the Nanjing Institute of Technology. Since 1990, he has been with Southeast University, Nanjing, China, first as an Associate Professor and then as a Professor. He was the Premier Foundation Investigator of the China National Science Foundation. From 1999 to 2002, he was the Principal Expert of the C3G Project, responsible for organizing China's 3G mobile communications research and development activities. From 2001 to 2006, he was the Principal Expert of the National 863 FuTURE Project. He has authored or coauthored more than 40 IEEE journal papers and two books in the areas of adaptive signal processing and neural networks and their applications to communication systems. His research interests include mobile communications, adaptive signal processing, and artificial neural networks with applications to communications and biomedical engineering. He is the recipient of the Excellent Paper Award from China Institute of Communications in 1987, and the Elite Outstanding Young Teacher Award from Southeast University in 1990, 1991, and 1993. He is currently the Chairman of the IEEE Nanjing Section.